Ann. Geophys., 30, 695–701, 2012
www.ann-geophys.net/30/695/2012/
doi:10.5194/angeo-30-695-2012

Annales Geophysicae

The emission of oxygen green line and density of O atom determined by using ISUAL and SABER measurements

H. Gao[1,2], **J.-B. Nee**[2], **and J. Xu**[1]

[1]State Key Laboratory of Space Weather, CSSAR, Chinese Academy of Sciences, Beijing, China
[2]Department of Physics, National Central University, Jhongli, Taiwan, China

Correspondence to: J.-B. Nee (jbnee@phy.ncu.edu.tw)

Received: 5 November 2011 – Revised: 28 March 2012 – Accepted: 31 March 2012 – Published: 19 April 2012

Abstract. Emissions of the 557.7 nm green line airglow observed by the ISUAL (Imager of Sprites and Upper Atmospheric Lightning) instrument on board the FORMOSAT-2 satellite in May and November 2008 are studied here to derive the density distributions of the atomic oxygen by using atmospheric parameters from MSISE-00 model and TIMED (Thermosphere Ionosphere Mesosphere Energetics and Dynamics)/SABER (Sounding of the Atmosphere using Broadband Emission Radiometry) measurements. The May observations were made in 10 days from a fixed orbit of longitude (100° E) with the results showing emission rate and O atom density both peaked at heights of about 90 km over 10° to 20° latitudes in the Northern Hemisphere (NH). In the Southern Hemisphere (SH), the emission rate and density of O atom are both low compared with those in NH. In November, the observations were made as the satellite traveled over all 14 orbits around the earth, covering all longitudes and latitudes of 25° S–45° N. Strong peaks of emission rates and O atoms are found at heights of about 95 km in the mid-latitudes in both hemispheres. In the equator, the airglow layer has a weaker emission rate but with higher altitude compared with those of mid-latitudes. In the lower and upper mesosphere at heights below 85 km and above 105 km, there are more O atoms in the equatorial regions than in the mid-latitudes. And there is a good correlation between the O atom and the temperature structure. A comparison with O atom distribution derived from OH airglow observed by TIMED/SABER at about the same time shows similar results.

Keywords. Atmospheric composition and structure (Airglow and aurora; Middle atmosphere – composition and chemistry; Pressure, density, and temperature)

1 Introduction

The green line emission at the wavelength 557.7 nm (hereinafter referred to as 558 nm) arising from the $O(^1S–^1D)$ transition is one of the prominent nightglow features in the mesosphere. The production of the excited oxygen atom $O(^1S)$ of an energy 4.2 eV was first proposed by Chapman in terms of a three body recombination of O atoms (Bates, 1988). However, a two-step mechanism involving an excited state of O_2 was proposed later by Barth (1961). The Barth Mechanism involves the following steps:

$$O + O + M \rightarrow O_2^* + M \quad \text{(R1)}$$

$$O + O_2^* \rightarrow O(^1S) + O_2. \quad \text{(R2)}$$

Studies of the green line and O atoms by various measurements have generally favored the Barth mechanism. Previous ground based and rocket measurements have provided useful information about the green line airglow, they are limited in spatial and time domains. The latest development of space instruments such as WINDII (Wind Imaging Interferometer) and SABER have provided extended information about the global and temporal variations of the airglow. For example, Zhang and Shepherd (1999) have shown green line had a midnight enhancement and peaked in mid latitudes based on WINDII observations. In the same study, they have found the OH Meinel band airglow peaked in the equator. In fact, OH airglow is also related to the chemistry of O atom through ozone by the chemical reaction

$$H + O_3 \rightarrow OH^* + O_2 \quad \text{(R3)}$$

with O_3 produced from O atom by the three body recombination process:

$$O + O_2 + M \rightarrow O_3 + M. \quad \text{(R4)}$$

Therefore, the measurements of OH airglow can also provide information about abundance of O atom. The difference in the latitudinal distributions of the O(^{1}S) and OH airglow reveals dynamic features governing their global distributions. A study of O atom from OH airglow observed by TIMED/SABER instruments is also studied in this paper to compare with results from green line airglow.

McDade et al. (1986) has discussed the mechanism for the production of the green line based on Reactions (R1) and (R2) and derived an expression of the emission rate with the following equation

$$V_{558\text{nm}} = A_{558\text{nm}}\left[\text{O}\left(^1\text{S}\right)\right] \quad (1)$$
$$= \frac{A_{558\text{nm}}\kappa_1[\text{O}]^3[\text{M}]}{\left\{\left(A\left(^1\text{S}\right)+\kappa_5[\text{O}_2]\right)\left(C'^{(0)}+C'^{(1)}[\text{O}]+C'^{(2)}[\text{O}_2]\right)\right\}}$$

where [] means number density, $V_{558\text{nm}}$ is the emission rate in photons $\text{cm}^{-3}\,\text{s}^{-1}$, [M] is the density of air including both O_2 and N_2. The rate constant with the three body recombination of O atoms is $\kappa_1 = 4.7\times10^{-33}(300/T)^2$, and the quenching rate of $\text{O}\left(^1\text{S}\right)$ by O_2 is $\kappa_5 = 2.32\times10^{-12}\exp((-812-1.82\times10^{-3}T^2)/T)$ (Capetanakis et al., 1993). In our study, the Einstein coefficients $A_{558\text{nm}}$ and $A(^1\text{S})$ are set as $1.26\,\text{s}^{-1}$ and $1.34\,\text{s}^{-1}$, respectively, which were given by Martin et al. (1999) and used in the study of Nakayama et al. (2006). Constants $C'^{(0)}$, $C'^{(1)}$ and $C'^{(2)}$ are given in McDade (1986).

From Eq. (1), we find $V_{558\text{nm}}$ is proportional to O atom to a cubic power: $[\text{O}]^3$. The rates k_1 and k_5 are temperature dependent such that the net emission rate is inversely related to the temperature while O atom is positively related to the temperature of the atmosphere. By measuring the emission rate at 558 nm, we should be able to derive the density of O atom with knowledge of the atmospheric temperature and density.

As we have discussed, the O atom can be studied by emissions of OH and O(^{1}S). In the past, Russell et al. (2003, 2004) have investigated the O atom distribution based on the green line data from WINDII measurements. Smith et al. (2010) have extensively studied the characteristic height of O atom over a region of 80–95 km by using the OH airglow measured by SABER instrument.

In this paper, we will study the green line and O atom distributions based on measurements made by the ISUAL instrument on board the FORMOSAT-2 satellite. In the next section, we will discuss the ISUAL instrument and measurements of the green line. In the third section, results of OI558 emission rate and distributions of O atoms are presented. Results of O atoms by using different atmospheric parameters and the derivation by using SABER OH airglow are discussed. Finally, a summary is given in the last section.

2 Instrument description and data processing

The ISUAL instrument on board the FORMOSAT-2 satellite was launched in May 2004 to a sun-synchronous orbit of 890 km with an inclination angle of 98.9°. The satellite has 14 orbits a day circling around the earth and can observe the same region of the atmosphere at a fixed latitude and longitude at the same local time. This type of observation provides a unique opportunity to study the upper atmosphere in detail compared with other non-sun-synchronous satellites which require months to return to the same local time at the same place.

The ISUAL instrument includes a CCD camera which looks through one of six interference filters to observe the atmospheric emissions in limb view (Nee et al., 2010). In this research, Filter #4 at 558 nm (FWHM 6 nm) is used to capture images of the green line airglow layer. The CCD takes 20 to 41 pictures of the atmosphere as the satellite travels along a specific orbit by looking out a distant window of 3300 km away. Each CCD picture has 524 (horizontal) × 128 (vertical) pixels corresponding to a window of 1200 km (width) × 270 km (height) of the upper atmosphere. A spatial resolution of about 2.14 km per pixel has been determined from the calibration.

Over the period of 7–16 May 2008, the green line was observed along the #10 orbit every night at midnight (local time). Forty one pictures were taken as the satellite traveled along this orbit. As an example, Fig. 1a gives a combined image of all 41 pictures to show a single layer of O(^{1}S) airglow observed on 10 May 2008. The observations started from the SH and ended in NH, covering latitudes of ∼11° S–20° N. The orbit 10 covers longitudes of about 98° E–107° E (briefly designated as 100° E in this paper). For the second green line observations for 1–2 November 2008, images have been taken along every orbit with orbits on 1 November from #9 to 14 and on 2 November from #1 to 8 and also #10. Therefore, these two day observations in November have covered all regions around the earth. The orbits which the satellite traveled to observe 558 nm airglow in this period are shown in Fig. 1b where one point on a track represents that one picture was recorded there. There are 21 pictures taken along every orbit (except the #14 orbit on Nov.1 and the #7 orbit on 2 November in which 20 pictures were taken because of orbit connectivity. In addition, on 2 November, the #10 orbit recorded 41 pictures).

By using an "onion-peel" process, the green line volume emission rate profiles can be retrieved from the images as described in Nee et al. (2010). Although there are 512 column pixels in one picture, we just use the 10 central column pixels to produce a profile of the emission rate. These emission rates are then used to calculate the O atom distributions by using Eq. (1) described in the first section.

The SABER instrument on board the TIMED satellite was launched in December 2001 to an altitude of 625 km with an inclination angle 74.1°. The satellite travels around the earth

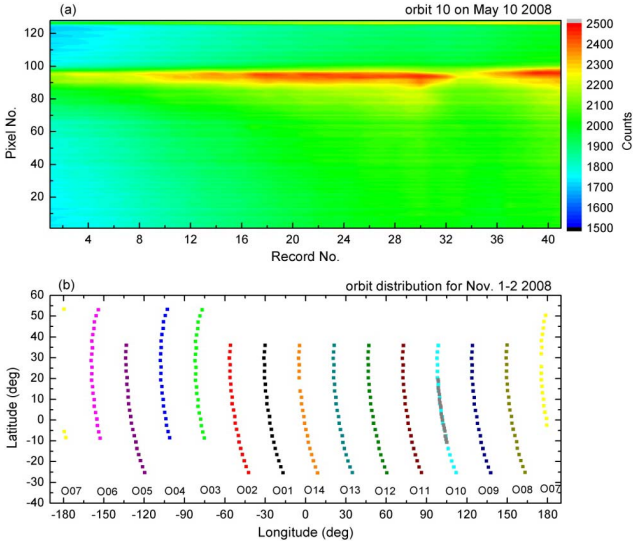

Fig. 1. **(a)** An image of a layer of O(^{1}S) airglow measured on 10 May 2008. **(b)** The latitudes and longitudes of ISUAL orbits. For 12 November 2008, one point in the figure represents one picture of the OI558 nm airglow emission was taken there.

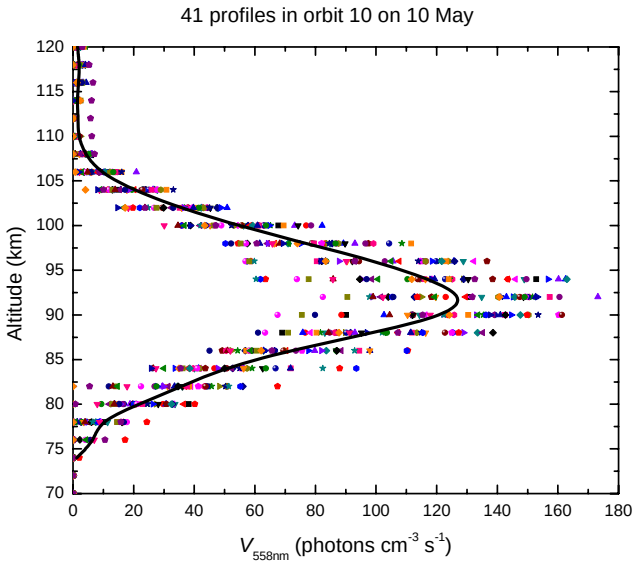

Fig. 2. Forty one scattered profiles of OI558 nm volume emission rate retrieved from images taken from orbit 10 on 10 May 2008. The 41 data are marked by different colors and symbols with the average profile in black solid line.

by about 15 orbits and takes about 60 days to cover the whole earth in every 24 h local time. The SABER instrument is a 10 channel infrared radiometer designed to measure the radiation, energy and structures of the MLT region (mesosphere and lower thermosphere). SABER observations cover from the winter hemisphere 53° to the summer hemisphere 83°. For every 58 s, SABER scans from 0 to 180 km to take atmospheric parameters including temperature, density, ozone density and OH airglow at the emission wavelengths 1.6 µm and 2.0 µm (see Russell et al., 1999). In this paper, we use the SABER 2.0 µm OH emission and ozone to derive the O atom by using the method introduced by Smith et al. (2010).

3 Results

3.1 558 nm emission rate

As an example, Fig. 2 shows the scattered diagrams of the height distributions of the emission rates derived from all 41 images measured on 10 May. Each image can derive a height profile separated by about 0.7° latitudes from the neighboring images. The black line in Fig. 2 is the average profile of all 41 data. From this figure we can see all data can fit a Gaussian distribution over a height range of 80–110 km with an average peak height of 92 km. As shown in Fig. 2, the peak height is quite stable for all data despite that the emission intensity can vary by about a factor of two. Such stable height distribution was not observed in OH airglow (Nee et al., 2010).

The peak height of O(^{1}S) airglow has been reported by many groups using different instruments (Zhang and Shepherd, 1999; Liu et al., 2008a; Yee et al., 1997; Skinner et al., 1998) and rocket measurements (Melo et al., 1996). The average peak height seems to be about 96 km. Our May observation shows a lower peak height of about 92 km. The difference may be related to the variations of airglow with the time, season and dynamics, as discussed extensively in Liu et al. (2008a) by using WINDII measurement. Long term studies show O(^{1}S) can vary between 84–104 km depending on the season and time (Liu et al., 2008a). The HRDI (High Resolution Doppler Imager) instrument also shows seasonal and local time variations of green line airglow (Skinner et al., 1998).

A contour diagram for green line in terms of height versus latitude can be made by averaging the emission rate in grids of 5 degree latitudes as shown in Fig. 3a and b for May and November data. For May data the measurements were made over a fixed longitude of about 100° E and latitudes of 10° S–20° N. We find the peak height is about 92 km and the peak emission in the NH is higher than that in the SH. For November data, the measurements were made over the latitudes of 25° S–45° N but over all longitudes. The results of averaging all longitudes gives a global distribution, showing green line emission at the equator is high in altitude but weak in intensity compared with those of mid-latitudes which have lower peak heights but stronger emission intensity. The two mid-latitude maxima are at about 95 km at 25° S and 93 km at 30° N with emission rates of 180 photons cm^{-3} s^{-1} and 240 photons cm^{-3} s^{-1}, respectively. Our results are basically consistent with WINDII/UARS data of Zhang and Shepherd (1999) who have shown OI558 nm emission rates are low near equator but high in the mid-latitudes for March 1992,

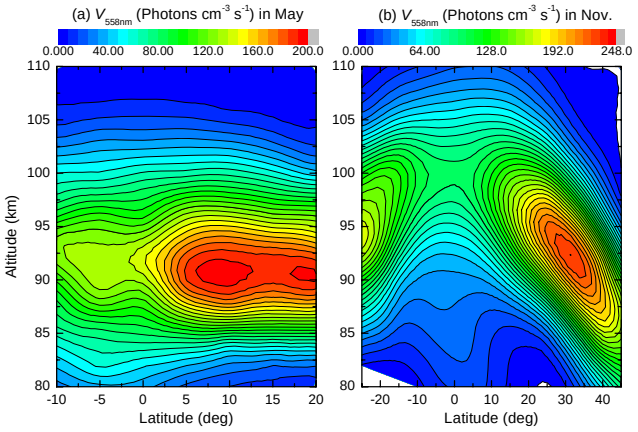

Fig. 3. The height-latitudinal distributions of green line emission rates observed by ISUAL in **(a)** May 2008 along orbit 10 (longitude ~100° E) and **(b)** November 2008 averaging over all longitudes.

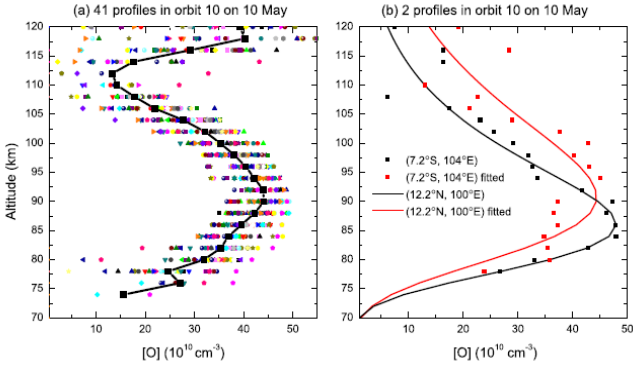

Fig. 4. **(a)** Height distributions of O atom derived from forty-one 558 nm emission rates observed along orbit 10 on 10 May 2008 (in different symbols and colors). The solid black line represents the average profile. **(b)** Two profiles of specific latitudes and longitudes (7.2° S, 104° E) and (12.2° N, 100° E) (doted lines), and their simulated results (solid lines) by using Eq. (2).

December 1992, and February 1993 at midnight conditions. We also find the magnitudes of the emission rates of ISUAL and WINDII data are close (Shepherd et al., 1999; Wang et al., 2002; Liu et al., 2008b).

We notice that the global measurement reveals a symmetric distribution with respect to the equator with the NH and SH peaks, appearing as mirror images of each other as shown in Fig. 3b. The symmetric distribution is also found in WINDII observation as shown in Zhang and Shepherd (1999).

3.2 Derivation of O atom density based on MSIS model

As discussed above, we can use the 558 nm emission rate to derive the density distribution of O atoms by using Eq. (1) with the knowledge of background atmospheric temperature and density. Russell et al. (2003, 2004) used the MSIS model to calculate O atom based on WINDII 558 nm data. We also used MSISE-00 model to derive O atom by using ISUAL OI 558 nm emission rate. We have selected the model calculations by using the same time and geological coordinates corresponding to the observations. Figure 4a shows 41 scattered diagrams of height distributions of O atom measured along the longitude 100° E corresponding to the emissions shown in Fig. 2. The average profile is shown as the solid black line. From Fig. 4a we can see O atom on 10 May has a peak at about 92 km and a minimum at about 112 km. O atom increases with altitude above 112 km, reaching a secondary peak above 120 km. However, we must be reminded there are also more errors at heights below 80 km and above 110 km where emission rates are low and standard deviations are high.

Based on results shown in Fig. 4a, the O atom distribution can be fitted with a Chapman profile as described in Eq. (2) below. This is the way Reed and Chandra (1975) and Melo et al. (2001) reported their distributions for the mesospheric O atoms:

$$[\mathrm{O}]_z = [\mathrm{O}]_{\max} \exp\{0.5[1-(z-h_{\max})/w] - \exp[-(z-h_{\max})/w]\}. \quad (2)$$

In Eq. (2), $[\mathrm{O}]_z$ is the atomic oxygen density at an altitude z; $[\mathrm{O}]_{\max}$ and $h_{\max}$ are the peak density and height of the atomic oxygen, respectively, and w is the width of profile.

By using Eq. (2), we have simulated the O atom distribution in 70–120 km by a least-square fit. In Fig. 4b, the dots are the height distributions of two observations at (7.2° S, 104° E) and (12.2° N, 100° E) and solid lines for the fitting results. In this figure, we find the height distributions of O atoms in the NH and SH are different, which should result from slightly un-symmetric distribution of airglow intensities in NH and SH, as can be seen in Fig. 3a.

It is known that MSISE-00 as an empirical model provides a good representation of the atmosphere in the region of middle to lower mesosphere but is not very accurate in the mesopause region (Xu et al., 2006). Recently by comparing the TIMED data with MSISE-00, Xu et al. (2006) have reported the deviations of MSISE-00 model. They also found inconsistency for cases of temperature inversions and some small scale deviations at different seasons.

3.3 Mesospheric temperatures based on SABER observations

We have employed TIMED/SABER temperature and density data as an alternative to the MSIS model for the calculations of O atom. One of the problems of using SABER measurements with ISUAL is related to their different orbits and observation strategies. It is rare that both satellites will be located at the same region to observe the same atmosphere

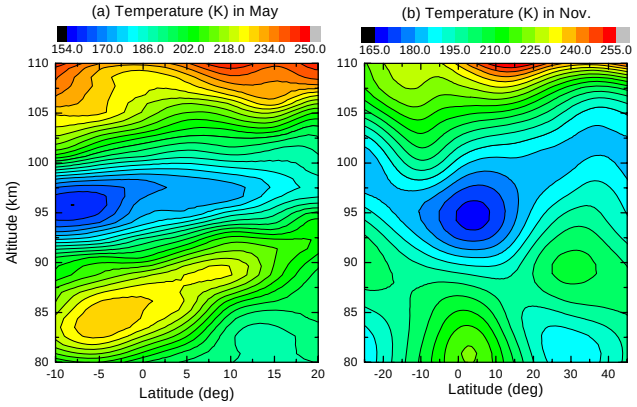

Fig. 5. SABER temperatures correspond to the same orbital conditions for **(a)** May and **(b)** November airglow observations.

at the same time. Fortunately, SABER observations were made around midnight in both periods of 7–16 May and 1–2 November 2008. We have therefore selected SABER observations for heights of 80–110 km during 7–16 May 2008 with the longitudes between 90° E and 110° E and during 1–2 November 2008 in all longitudes in the time interval of −02:00 LT to 02:00 LT local time to construct bins of 5 degree latitudes. We then used ISUAL OI 558 nm emission rate to calculate O atom density within these bins.

We will first look at the SABER temperature data since it is an important parameter in the calculations. Figure 5 shows contour diagrams of SABER temperatures for both May and November in 2008. We find from Fig. 5a the mesopause in May is located at about 97 km with a low temperature of about 160 K. Below the mesopause, there is a warm layer with a local temperature maximum of about 220 K at about 83 km at 10° S. The height of this warm layer increases to 92 km at 20° N. Higher temperatures also appear above 105 km.

For November, the temperature structure shows a complex pattern in terms of multiple highs and lows. The mesopause height is at 95 km over the equatorial region and increases to about 100 km at mid-latitudes in the SH and NH as shown in Fig. 5b. In the lower mesosphere at about 85 km, the temperature in the equatorial region is higher than those in the mid-latitudes. But in the upper mesosphere at heights 100–110 km, there is a warm layer corresponding to the thermosphere. In November, high temperatures in the mesosphere can be found in three regions: 81 km over the equator, 90 km at both 25° S and 30° N. The highest temperature appears above the mesosphere at 110 km at 10° N.

By comparing Fig. 5b with Fig. 3b, we can see the stronger 558 nm airglow layer lies near the mesopause. We must be reminded that emission is negatively correlated and O atom is positively correlated with temperature as given in Eq. (1), so that peak emission and O atom are correlated with cold and warm regions, respectively.

3.4 O atom based on SABER observations

By using SABER temperature and density data in Eq. (1), we have calculated O atom distributions for May and November with results shown in Fig. 6. Figure 6a indicates a layer of O atoms exists in May at 85–95 km with the peak height increasing with latitude even though the emission rate is relatively unchanged in height distribution as shown in Fig. 3a. This difference should be attributed to the temperature distribution as shown in Fig. 5a. The number density of O atoms in the NH is more and higher than those in the SH. A maximum of O atom appears at 10° N at 90 km. Besides these trends, there is a low value of O atom at about 95 km at 10° S in the SH related to the temperature conditions shown in Fig. 5a.

In November, O atom shows several maxima and minima in different heights and latitudes. Below 85 km, more O atoms are found at the equator than other regions. In the mid-latitudes there are two minima found at about 25° S/N. In the region of 85–100 km, there is a peak of O atom at about 93 km at 30° N. The corresponding peak in the SH should lie at 30° but was partially cut in the diagram. These two mid-latitude peaks form mirror images similar to the emission double shown in Fig. 3b. A major peak of O atom is located at about 10° N at 110 km, and a secondary peak at 10° S at 104 km. The last two peaks lying above 100 km are correlated with the temperature structure in this region as can be seen in Fig. 5b. The secondary peak at 10° S may be a split from the major peak.

In terms of absolute number density, O atoms in May or November are both in the level of 10^{11} cm^{-3} which is close to other results reported in the literatures (e.g. Smith et al., 2010; Russell et al., 2003). We also calculated the volume mixing ratio (vmr) of O. The altitude–latitude distribution of the vmr below 100 km is very similar to the calculations of Smith et al. (2010) who used SABER OH(2.0 µm) airglow to derive the O atom density and mixing ratio. In addition, our results indicate that the O atom at 10° N (109 km) has a mixing ratio about 0.4 compared with less than 0.3 at all other latitudes and heights.

3.5 Discussion

Following Smith et al. (2008, 2010) and using the new coefficients given by Xu et al. (2012), we also calculated the O atoms in the 80–100 km height region based on SABER OH(2.0 µm) airglow emission rate and ozone density measured in the period of 7–16 May 2008 in −02:00–02:00 LT and in longitudes 90° E–110° E. Another calculation has been made for 1–2 November 2008 at −02:00–02:00 LT but over all longitudes. The altitude–latitude distribution of the O atom retrieved from SABER May data shows O atoms peaks over the latitudes 10° S–20° N and heights 80–100 km similar to what are displayed in Fig. 6a. There are more O atom in the NH than the SH and the peak height increases in general toward mid-latitudes in the NH. SABER data also

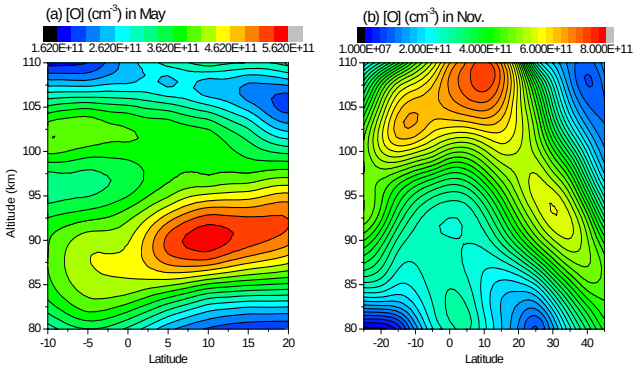

Fig. 6. Atomic oxygen density in latitude-height contour for **(a)** May and **(b)** November.

find low O atoms in the SH and equator at about 95 km. For SABER November data over the latitudes 25° S–45° N and heights above 85 km, peak O atoms are lying higher but with less density in the equator than those in the mid-latitudes similar to what is shown in Fig. 6b. Below 85 km, O atom has higher density in the equatorial region than that at mid-latitudes. SABER results also show O atom density is in the level of 10^{11} cm^{-3}.

We also analyzed the altitude–latitude distributions of O atom derived from the green line emission by using the atmospheric density and temperature from MSISE-00 model. The results indicate the distributions in both May and November are generally similar to those derived based on SABER observations as shown in Fig. 6. Meanwhile some small differences exist. For example, calculations made with MSISE-00 model show constant altitudinal and latitudinal variations of O atom density and there is not a low density region around 95 km in the SH in May. This can be attributed to that there is not such structure in the distribution of temperature from MSISE-00 model.

It is worth mentioning that two coefficients $C'^{(1)}$ and $C'^{(2)}$ in Eq. (1) are taken as 211 and 15 in our study. In fact, McDade et al. (1986) got four different sets of values for the two coefficients by fitting the green line emission rate profiles from ETON rocket experiments using Eq. (1). In the fitting, they used four different sets of [O] which were obtained based on the [O] from CIRA 1972 and MSIS-83 atmospheric models, respectively. In this work, we use the values of $C'^{(1)}$ and $C'^{(2)}$ obtained based on MSIS-83 model. However, the atmospheric temperature and density from MSISE-00 model and SABER are used, which are different from MSIS-83 model. We will discuss the uncertainty in the derivation of [O] using new data and model due to the values of $C'^{(1)}$ and $C'^{(2)}$ from MSIS-83 model.

According to the maximum and minimum of $C'^{(1)}$ and $C'^{(2)}$ given in Table 3 of McDade et al. (1986), we assume $C'^{(1)}$ and $C'^{(2)}$ decreasing by 10 % and 30 %, which means $C'^{(1)}$ and $C'^{(2)}$ are set as 0.9 $C'^{(1)}$ and 0.7 $C'^{(2)}$, respectively.

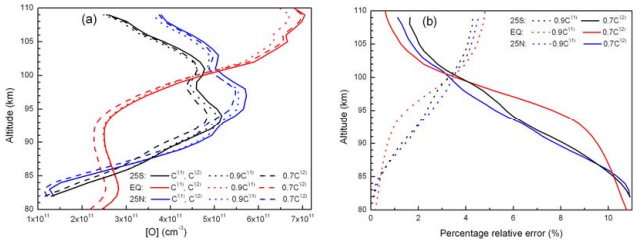

Fig. 7. (a) Altitudinal distributions of [O] at three latitudes derived by using three sets of values: $C'^{(1)}$ and $C'^{(2)}$, 0.9 $C'^{(1)}$ and $C'^{(2)}$, $C'^{(1)}$ and 0.7 $C'^{(1)}$, and **(b)** the percentage errors of [O] derived by using the second and third sets of coefficients.

We use the new values to derive the [O] at three latitudes: 25°N/S and the equator, by using the atmospheric temperature and density from SABER. We also calculate the percentage errors as follows:

$$100\,\% \times \left|[\mathrm{O}]_{0.9C'^{(1)},C'^{(2)}} - [\mathrm{O}]_{C'^{(1)},C'^{(2)}}\right| / [\mathrm{O}]_{C'^{(1)},C'^{(2)}}\,, 100\,\% \times \left|[\mathrm{O}]_{C'^{(1)},0.7C'^{(2)}} - [\mathrm{O}]_{C'^{(1)},C'^{(2)}}\right| / [\mathrm{O}]_{C'^{(1)},C'^{(2)}}\,.$$

The results are shown in Fig. 7a and b. From this figure, we can see that the derived [O] decreases with $C'^{(1)}$ or $C'^{(2)}$, decreasing at all altitudes and latitudes. And all uncertainties of [O] are less than 11 % as shown in Fig. 7b.

4 Summary

By using the ISUAL instrument on board the sun-synchronous satellite FORMOSAT-2, the images of the OI 558 nm green line airglow emission was measured on 7–16 May 2008 and 1–2 November 2008. The profiles of OI 558 nm emission rates are derived from the observation by using an "onion-peel" process. Furthermore, the O atom density profiles are retrieved from the OI 558 nm emission rates by using atmospheric temperature and density from SABER and MSISE-00 model, respectively.

The May 2008 observation made at an averaged longitude of 100° E shows emission rates peaked at about 92 km over the latitudes 10° S–20° N. The retrieved O atoms have peak heights increasing toward the NH. Both the emission rate and O density are higher in NH.

For 1–2 November 2008, ISUAL observations were made globally by traveling over all longitudes and a latitude range of 25° S–45° N. In November, the OI 558 nm emission rates and O atoms show double maxima at about 95 km in the mid-latitudes. The double peaks at mid-latitudes are symmetrically distributed with respect to the equator. In the equatorial region, peak O atom density was found around 10° N at 110 km in the lower thermosphere. In the lower mesosphere around 82 km, there are double minima of O atoms in the mid-latitudes also symmetrically located.

We also calculate O atom by using SABER OH airglow. The results show similar distribution to that from ISUAL green line observations.

Acknowledgements. We thank the FORMOSAT-2 and TIMED/SABER science teams for providing the data used in this study. GH wishes to thank National Science Council for postdoctor position at NCU. This research is supported through a grant: NSC100-2811-M-008-004. This work is supported by the Chinese Academy of Sciences (KZZD-EW-01-2), the National Science Foundation of China (41004062, 40921063, 40890165) and the National Important Basic Research Project of China (2011CB811405). The project is also supported by the Specialized Research Fund for State Key Laboratories.

Topical Editor C. Jacobi thanks two anonymous referees for their help in evaluating this paper.

References

Barth, C. A. and Hildebrandt, A. F.: The 5577 A airglow emission mechanism, J. Geophys. Res., 66, 985–986, 1961.

Bates, D. R.: Excitation of 557.7 nm OI line in nightglow, Planet. Space Sci., 36, 883–889, 1988.

Capetanakis, F. P., Sondermann, F., Höser, S., and Stuhl, F.: Temperature dependence of the quenching of O(1S) by simple inorganic molecules, J. Chem. Phys., 98, 7883–7887, 1993.

Liu, G., Shepherd, G. G., and Roble, R. G.: Seasonal variations of the nighttime O(1S) and OH airglow emission ratesat mid-to-high latitudes in the context of the large-scale circulation, J. Geophys. Res., 113, A06302, doi:10.1029/2007JA012854, 2008a.

Liu, G., Shepherd, G. G., and Tepley, C. A.: Variations of the tropical O(1S) nightglow as observed with the Arecibo Observatory photometer and WINDII on UARS, J. Atmos. Sol.-Terr. Phys., 70, 1309–1317, 2008b.

Martin, W. C., Fuhr, J. R., Kelleher, D. E., Musgrove, A., Podobedova, L., Reader, J., Saloman, J. E. B., Sansonetti, C. J., Wiese, W. L., Mohr, P. J., and Owen, K.: NIST Atomic Spectra Database (version 2.0), National Institute of Standards and Technology, Gaithersburg, MD, available at: http://physics.nist.gov/asd, 1999.

McDade, I. C., Murtagh, D. P., Greer, R. G. H., Dickinson, P. H. G., Witt, G., Stegman, J., Llewellyn, E. J., Thomas, L., and Jenkins, D. B.: ETON 2: Quenching parameters for the proposed precursors of O2(b1Σg+) and O(1S) in the terrestrial nightglow, Planet. Space Sci., 34, 789–800, 1986.

Melo, S. M. L., Takahashi, H., Clemesha, B. R., Batista, P. P., and Simonich, D. M.: Atomic oxygen concentrations from rocket airglow observations in the equatorial region, J. Atmos. Terr. Phys., 58, 1935–1942, 1996.

Melo, S. M. L., McDade, I. C., and Takahashi, H.: Atomic oxygen density profiles from ground-based nightglow measurements at 23° S, J. Geophys. Res., 106, 15377–15384, 2001.

Nakayama, T., Takahashi, K., Matsumi, Y., and Fujiwara, H.: Laboratory study of O(1S) formation process in the photolysis of O_3 and its atmospheric implications, J. Atmos. Chem., 53, 107–122, 2006.

Nee, J.-B., Tsai, S.-D., Peng, T.-H., Hsu, R.-R., Chen, A. B.-C., Zhang, S., Huang, T.-Y., Rajesh, P. K., Liu, J.-Y., Frey, H. U., and Mende, S. B.: OH Airglow and Equatorial Variations Observed by ISUAL Instrument on Board the FORMOSAT-2 Satellite, Terr. Atmos. Ocean. Sci., 21, 985–995, 2010.

Reed, E. I. and Chandra, S.: The Global Characteristics of Atmospheric Emissions in the Lower Thermosphere and Their Aeronomic Implications, J. Geophys. Res., 80, 3053–3062, 1975.

Russell, J. M., Mlynczak, M. G., Gordley, L. L., Tansock, J., and Esplin, R.: An overview of the SABER experiment and preliminary calibration results, Proc. SPIE Int. Soc. Opt. Eng., 3756, 277–288, 1999.

Russell, J. P. and Lowe, R. P.: Atomic oxygen profiles (80–94 km) derived from Wind Imaging Interferometer/Upper Atmospheric Research Satellite measurements of the hydroxyl airglow: 1. Validation of technique, J. Geophys. Res., 108, 4662, doi:10.1029/2003JD003454, 2003.

Russell, J. P., Lowe, R. P., and Ward, W. E.: Atomic oxygen annual and semi-annual variations in the mesopause region for mid and equatorial latitudes, J. Atmos. Sol.-Terr. Phys., 66, 451–461, 2004.

Shepherd, G. G., Zhang, S., and Wang, X.: Variability in MLT dynamics and species concentrations as observed by WINDII, Earth Planets Space, 51, 845–853, 1999.

Skinner, W. R., Yee, J.-H, Hays, P. B., and Burrage, M. D.: Seasonal and local time variations in the O(1S) green line, O2 atmospheric band, and OH Meinel band emissions as measured by the High Resolution Doppler Imager, Adv. Space Res., 21, 835–841, 1998.

Smith, A. K., Marsh, D. R., Russell III, J. M., Mlynczak, M. G., Martin-Torres, F. J., and Kyrölä, E.: Satellite observations of high nighttime ozone at the equatorial mesopause, J. Geophys. Res., 113, D17312, doi:10.1029/2008JD010066, 2008.

Smith, A. K., Marsh, D. R., Mlynczak, M. G., and Mast, J. C.: Temporal variations of atomic oxygen in the upper mesosphere from SABER, J. Geophys. Res., 115, D18309, doi:10.1029/2009JD013434, 2010.

Wang, D. Y., Ward, W. E., Solheim, B. H., and Shepherd, G. G.: Longitudinal variations of green line emission rates observed, J. Atmos. Sol.-Terr. Phys., 64, 1273–1286, 2002.

Xu, J., Ji, Q., Wei, Y., and Ma, R.: Comparison between the TIMED observed global temperature distribution and the MRLMSISE-00 empirical atmospheric model, Chin. J. Space Sci., 26, 177–182, 2006 (in Chinese).

Xu, J., Gao, H., Smith, A. K., and Zhu, Y.: Using TIMED/SABER nightglow observations to investigate hydroxyl emission mechanisms in the mesopause region, J. Geophys. Res., 117, D02301, doi:10.1029/2011JD016342, 2012.

Yee, J.-H., Crowley, G., Roble, R. G., Skinner, W. R., Burrage, M. D., and Hays, P. B.: Global simulations and observations of $O(^1S)$, $O_2(^1\Sigma)$ and OH mesospheric nightglow emissions, J. Geophys. Res., 102, 19949–19968, doi:10.1029/96JA01833, 1997.

Zhang, S. P. and Shepherd, G. G.: The influence of the diurnal tide on the $O(^1S)$ and OH emission rates observed by WINDII on UARS, Geophys. Res. Lett., 26, 529–532, doi:10.1029/1999GL900033, 1999.